p Doping in Expanded Phases of ZnO: An Ab Initio Study

D. Hapiuk, Miguel A. L. Marques, P. Melinon, Jose A. Flores-Livas, Silvana Botti, Bruno Masenelli

p-doping in expanded phase of ZnO: an *ab initio* study

D. Hapiuk,[1,*] M. A. L. Marques,[1] P. Melinon,[1] J. A. Flores-Livas,[1] S. Botti,[1] and B. Masenelli[2]

[1] *Université de Lyon, F-69000, France; Univ. Lyon 1, Laboratoire PMCN; CNRS, UMR 5586; F69622 Villeurbanne Cedex*

[2] *Université de Lyon, F-69000, France; Institut des Nanotechnologies de Lyon; UMR 5270 CNRS and INSA Lyon, 7 avenue Jean Capelle, 69621 Villeurbanne CEDEX, France*

(Dated: January 16, 2012)

The issue of p-doping in nanostructured cage-like ZnO is investigated by state-of-the-art calculations. Our study is focused on one prototypical structure, namely sodalite, for which we show that p-type doping is possible for elements of the V, VI, and VII columns of the periodic table. However, some dopants tend to form dimers thus impairing the stability of this kind of doping. This difference of behavior is discussed and two criteria are proposed to ensure stable p-doping.

PACS numbers: 66.30.-h; 71.15.Mb; 71.20.Nr; 61.46.-w

The interest in ZnO has greatly increased over the last decade due to its remarkable properties. Its excitonic UV luminescence and high excitonic binding energy (60 meV) should enable nanometric scaled applications such as biological tracers [1], UV laser diodes [2] and polariton lasers, or integration in solar cells with high efficiency. In this context, the electronic properties of ZnO, and more specifically the possibilities for doping, hold a particular interest. However, unlike n-type doping, p-type doping is a real problem for this material, therefore limiting its use for electronic applications. This behavior arises from a variety of causes including native crystalline defects and impurity incorporations [3]. Many attempts have been made to p-dope wurtzite ZnO samples but sound achievements are scarce [4]. These difficulties could be circumvented by exploring other ZnO phases that have been proposed in recent years [5–8]. Of particular interest are cage-like structures that are particularly suited for endohedral doping. Such phases have been recently proposed for hydrogen purification membranes [9] and have been shown to exhibit a transient p-type doping due to the free motion of H atoms in the network [9]. Furthermore, cage-like endohedral doping has proved to be an interesting method used in other semiconductor materials. For instance, in Si clathrates endohedral doping by alkaline atoms allows the control of the electronic properties [10] up to the appearance of superconductivity [11]. It is thus relevant to investigate the possibilities of endohedral doping in ZnO cage-like materials in the hope to achieve p-doping.

In this letter, we investigate endohedral p-doping of a particular ZnO cage-like structure, namely the sodalite structure (SOD, according to the nomenclature of the International Zeolite Association). This turns out to be the simplest and most symmetric binary structure of the cage-like family, and is the unique solution to the Kelvin problem for binary compounds [12]. It consists of a regular stacking of truncated octahedra which are Archimedean solids with 14 faces (8 regular hexagons and 6 squares) leading to the net formula $(ZnO)_{12}$ (see inset in Fig. 1). Furthermore, even though the ZnO sodalite structure has not been experimentally synthesized, theoretical [13] and experimental works [14] tend to show that its building block, the $(ZnO)_{12}$ cluster, is stable and energetically favored. Furthermore, a 25% co-substituted cage-like structure (the ATN phase) has been obtained by a solid state reaction [15]. These results point to the possibility of growing cage-like expanded phases of II-VI semiconductors, and in particular of ZnO.

TABLE I: Cohesion energy difference ΔE and volume for several cage-like structures [5–8] obtained from DFT calculations. The lattice and coordinates parameters were obtained from Ref. 29.

Name	Space group	ΔE(eV/ZnO)	Volume(Å^3/ZnO)
wurtzite	$P63mc$	0	24.85
SOD	$Pm\overline{3}n$	+0.132	30.42
BCT	$I4/mmm$	+0.029	25.99
ATV	$Abm2$	+0.137	26.38
AFI	$P6cc$	+0.189	30.61
LTA	$Pm\overline{3}m$	+0.248	36.87
ATN	$I4/mmm$	+0.277	26.56
VFI	$P63/mcm$	+0.291	37.34
rocksalt	$Fm3m$	+0.297	20.43

To study the stability and the electronic structure of sodalite we used first principles calculations within the density-functional theory (DFT) formalism and with a plane-wave pseudopotential approach (using the VASP code [16]). We used the Perdew-Burke-Ernzerhof (PBE) exchange-correlation functional [17] and the projector augmented-wave description of the electron-ion interaction [22]. Brillouin zone integrals were converged with a 600 eV plane-wave cutoff and a $2 \times 2 \times 2$ Monkhorst-Pack k-point mesh, using the tetrahedron method with Blöchl corrections. The relaxation was performed with the standard conjugated gradient algorithm. This calculation procedure is common to all the results presented in this work unless otherwise stated.

From all known cage-like ZnO structures [8], the so-

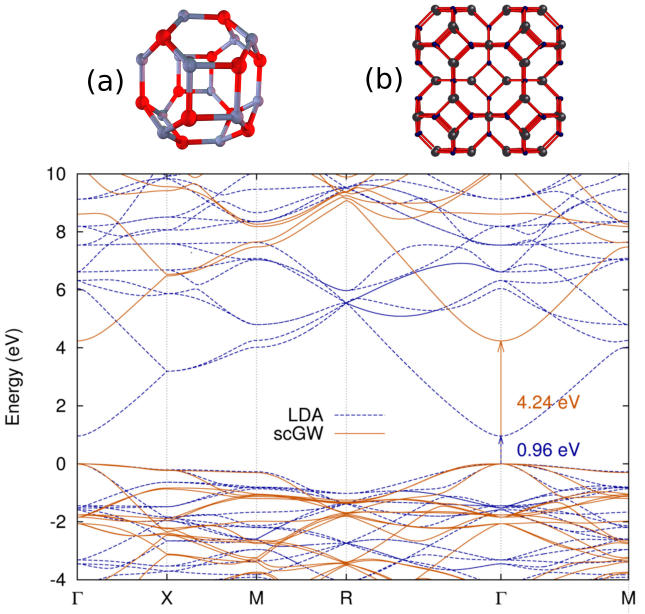

FIG. 1: Band structure of ZnO sodalite structure in DFT-LDA and sc-*GW*. The gap is direct at Γ and estimated to be 4.2 eV in sc-*GW* and 0.9 eV in LDA. The inset (a) presents an elementary cage of the sodalite illustrated in inset (b).

dalite has a relatively low energy, with a cohesion energy of -8.972 eV per unit of ZnO (see Table I), when calculated as the difference between the energy of sodalite and of isolated atoms. It is 132 meV higher than the energy of wurtzite but also 165 meV lower than that of rocksalt, the latter structures being the only naturally occurring phases. This result is consistent with previous calculations [9] and further justifies the choice of the sodalite as a potential candidate for the study of endohedral *p*-doping.

It is true that the *ab initio* determination of the quasiparticle band-structure of ZnO poses a quite complicated problem as standard methods, such as DFT or even standard (perturbative) G_0W_0, yield bandgaps that are much smaller than the experimental value [18, 21]. To obtain the best possible band-structure for the ZnO sodalite (cf. Fig. 1) we have to go beyond these methods [19, 20]. In this work, we used a state-of-the-art approach based on a restricted self-consistent (sc) *GW* scheme. Such an approach, that we will refer to as sc-*GW*, consists in performing a self-consistent *GW* calculation within the Coulomb hole plus screened exchange (COHSEX) approximation [28], followed by a perturbative *GW* step on top of it. This method has been applied to many transition-metal compounds, yielding excellent results for the bandgaps and the quasiparticle band structure [23–25]. The sc-*GW* calculations were performed using the code ABINIT [26]. We included semicore states in the valence to build the norm-conserving pseudopotentials for Zn, and used a 3x3x3 sampling of the Brillouin zone. The absolute value of the sc-*GW* direct bandgap at Γ has however to be interpreted with care. In fact, for wurtzite ZnO (experimental gap 3.3 eV), our method yields a direct band gap at Γ of 4.4 eV, while the local-density approximation (LDA) yields 0.82 eV and standard *GW* 2.1 eV. The overestimation of the gap by sc-*GW* can probably be explained by the neglect of the contribution of phonons to the screening, that can have a very large effect in ionic oxide materials [27]. On the other hand, for ZnO sodalite, we obtain a sc-*GW* direct band gap at Γ of 4.2 eV (Fig. 1), while LDA yields 0.96 eV and standard G_0W_0 2.5 eV. By comparing the two structures, and by assuming that sc-*GW* is our best theoretical estimate, it becomes clear that the experimental gap of ZnO sodalite is direct at Γ and is very likely lower than the one of the wurtzite structure by 0.1–0.3 eV, i.e., in the range 3.2–3.4 eV. The ZnO sodalite thus retains the interesting feature of the wurtzite ZnO for the UV opto-electronic applications and motivates the study of its doping properties.

TABLE II: Cohesion energy of 7% doped ZnO sodalite and features of 1% doped ZnO sodalite, including the presence of Jahn-Teller effect (JT), the proportion of hybridization at the Fermi level and the presence of dimerization.

Dopant	$E_{cohesion}(eV/ZnO)$	JT	hybrid	dimerization
O	-9.393	No	26.1%	No
F	-9.439	No		No
Cl	-9.171	No		No
Br	-9.067	No		No
Te	-9.072	No	43.8%	No
I	-8.939	No		No
H	-9.130	Yes	20.1%	Yes
N	-9.293	Yes	37.8%	Yes
P	-9.194	No	47.7%	Yes
S	-9.173	No	45.3%	Yes
Se	-9.136	Yes	46.9%	Yes

To study *p*-doping, we used elements of the V, VI, and VII columns of the periodic table, with atomic concentrations of the doping element varying from 1% to 14% (i.e., every cage is filled). Table II presents the cohesion energies of the ZnO sodalite doped with different dopants for a 7% concentration (i.e., every other cage is filled). The doped ZnO sodalite is always more stable than the undoped one indicating hybridization with the dopant. With F, the absolute value of the cohesion energy of the structure reaches the maximum of 335 meV/ZnO higher than the undoped ZnO sodalite. This result indicates that the dopant could be useful to ease the synthesis of the ZnO sodalite just as it is the case for Si clathrates [30]. The cohesion energy naturally varies with regard to the nature of the dopant (Table II).

Clearly, the electronic properties are also dependent on the dopant. Figure 2 presents the DOS of the undoped ZnO sodalite along with the DOS of the structure doped

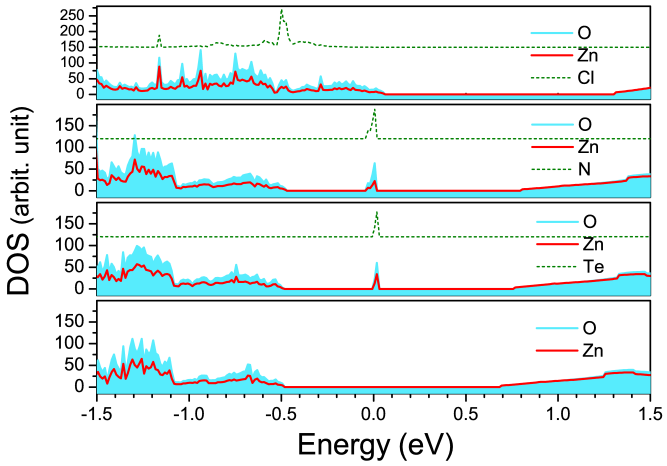

FIG. 2: Electronic density of states of N, Cl, and Te doped ZnO sodalite projected on the states of the constituents. The Fermi level is located at 0 eV. The contribution of each atom is respectively: Zn (blue), O (red) and N, Te, and Cl (green). The dopant states are strongly localized near the top of the valence band. The DOS of pure ZnO sodalite is pictured in the bottom panel. The DOS of the different conduction bands has been multiplied (×10) for the sake of visibility as well as the contribution of Cl (×5). The dopant atomic concentration is 1%.

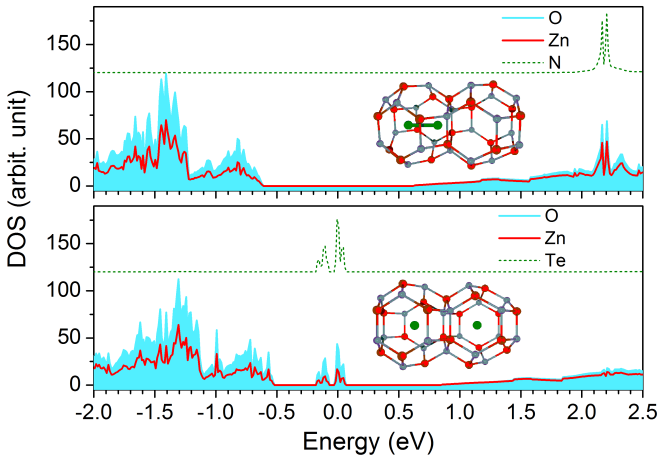

FIG. 3: Electronic density of states of N and Te doped ZnO sodalite projected on the states of the constituents. The Fermi level is located at 0 eV. Two dopants are placed in two neighboring cages of the ZnO sodalite, and the insets illustrate the position of the atoms after relaxation. The DOS of the different conduction bands has been multiplied (×5) for the sake of visibility as well as the contribution of the N and Te dopants (×2). The dopant atomic concentration is 2%.

with N, Cl, and Te. In all cases, the dopant atomic concentration is nearly 1% [N@$(ZnO)_{48}$, Te@$(ZnO)_{48}$, and Cl@$(ZnO)_{48}$]. All are *p*-type doped as it is well evidenced by the position of the Fermi level at 0 eV. In the case of N and Te doped ZnO sodalite, the total eDOS at this particular point has an equal contribution from O and N (or Te) states and a smaller contribution from Zn states. The proportion of hybridization of the states at the Fermi level has also been calculated. This proportion has been defined as the ratio of the DOS projected on the dopant states with the total DOS at the Fermi level. A value of 0% or 100% means a pure transfer of electrons from the dopant to the electronic states of the ZnO network. This scheme is close to the conventional scheme of a hydrogen-like impurity in substitutional doping. Conversely, a value around 50% means a strong hybridization between the orbitals of the dopant and the network. The results are presented in Table II. Interestingly, all values are close to 50%, which implies that the insertion of the dopant in the ZnO sodalite cages induces a strong hybridization. As for the Cl doped ZnO sodalite, it presents a degenerate state. This means that the dopant concentration is high enough to strongly perturb the eDOS of the doped sodalite. This latter is no longer a classic doped semi conductor but presents a metallic behavior. This transition between a doped semi conductor and a degenerate semi conductor is also known as the Mott transition [31] and occurs for a critical dopant concentration. Thus, the hybridization is very strong and perturbs the valence band near the Fermi level. Clearly, the critical concentration for the Mott transition depends on the nature of the dopant.

It is also pertinent to study the constraints induced by the dopant on the framework. For example, the equilibrium position of the Te atom is at the center of the cage and the lattice is only slightly affected by doping. Indeed, according to our calculations, the diameter of a cage of the undoped ZnO sodalite is 6.34 Å against 6.47 Å for the Te doped one. On the contrary, the N atom moves spontaneously away from the center of the cage, exhibiting a Jahn-Teller effect leading to an equilibrium position shifted by 1.37 Å and a lattice more deformed locally around the dopants (the cage containing the dopant is deformed and its diameter varies between 6.16 Å and 6.55 Å). The shifted distance due to the Jahn-Teller effect is of the same order of magnitude as the one reported for the $Na@Si_{28}$ silicon clathrate [10].

We also performed calculations for several other *p*-type dopants, as listed in Table II. For ZnO sodalite doped with Cl, Br and I, a dopant concentration of 1% is already enough to lead to a degenerate semiconductor with the Fermi level localized in the valence band. For the other dopants, the Mott transition appears at higher concentrations. We also notice a Jahn-Teller effect for the light elements, i.e. H, N, O, and F. The inspection of the lattice distortion around the atoms which present a Jahn-Teller effect reveals a repulsion between O and the dopant, while Zn atoms remain at their initial positions.

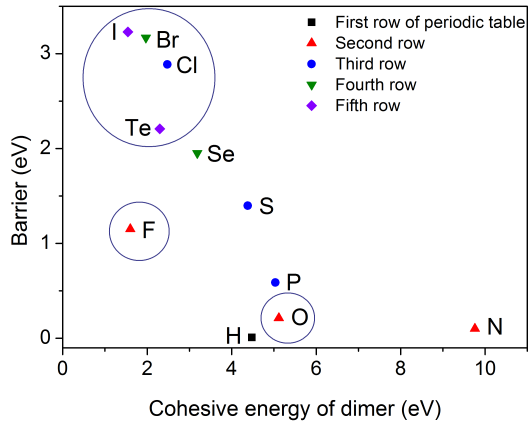

FIG. 4: Magnitude of the energy barrier in doped ZnO sodalite as a function of the cohesion energy of the dimer. The circled areas point the dopants which do not dimerize. Each symbol corresponds to a different row of the periodic table.

Since two adjacent cages may be occupied by doping atoms, it may be possible that those atoms dimerize. Figure 3 displays the case of Te and N doping. For that purpose, we start with two atoms in two adjacent cages [The dopant atomic concentration is thus 2% with the stoichiometry $N@(ZnO)_{24}$] and relax the system with the conjugated gradient algorithm. As a result, Te stays at the center of the cage while N moves spontaneously to form a N_2 dimer. In the latter case, we obtain a set of two independent lattices formed by the ZnO sodalite and N_2 molecules. This is well evidenced by the sharp peaks in the DOS due to N in the conduction band far away from the Fermi level. Thus, the ZnO sodalite is not p-doped any more. The new equilibrium state exhibits a mean distance of $d_{\text{N-N}} = 1.11\,\text{Å}$, close to the experimental bond length of the dimer $d_{\text{N-N}} = 1.10\,\text{Å}$. This result can be obtained for other elements, like H, N, P, S, and Se, while O, F, Cl, Br, Te and I do not dimerize and preserve p-like doping at any concentration.

Eventually, the diffusion of the dopant is of outmost importance for the ZnO sodalite synthesis. To study this problem, we calculated the magnitude of the energy barrier when the dopant moves along the [111] direction crossing the shared hexagon, see Fig. 4. The magnitude of the energy barrier is calculated between the equilibrium position of the dopant and the position where the dopant crosses the hexagonal face separating two cages. Globally, the energy barrier increases with the atom size, in agreement with steric hindrance. However, this is not the only criterion. One has also to consider the magnitude of the interaction of the guest atom with the host lattice. The interaction becomes stronger as the p valence shell of the guest atom is filled, requiring the transfer of fewer electrons to fulfill the octet rule. Considering elements belonging to the same row of the periodic table, for instance N, O and F, one can see that the magnitude of the energy barrier increases from N to F, almost independently of the atomic radius. The elements which do not dimerize (circled areas in Fig. 4) exhibit a high value for the energy barrier and a weak cohesion energy of the dimer. These two criteria allow to discriminate the dopants that dimerize from those that do not. Consequently these criteria can predict a stable or unstable p-type doping. The case of O is an exception since, in spite of the large cohesion energy of its dimer and the small value of the energy barrier, it does not dimerize. The absolute energy barrier is relatively large compared to the thermal energy and questions the efficiency of the diffusion. We did the same calculations for the Na-doped silicon type II clathrate where diffusion is observed at moderate temperature ($T < 600\,\text{K}$) [32]. This energy barrier is estimated to be 2.14 eV, similar to the ones found in ZnO sodalite.

In conclusion, using state-of-the-art DFT calculations we showed that endohedral doping of cage-like structures is a promising method for the achievement of p-doping in ZnO, even up to degenerate levels. Since doping in endohedral sites induces less stress than substitutional doping, all elements of the V, VI, VII columns of the periodic table are eligible. However some of them dimerize, and therefore do not lead to p-doping. In particular, the case of N, that is thoroughly discussed in the literature in the context of substitutional doping, does not seem to be the best candidate for endohedral doping. Other elements such as O, F, Cl, Br, Te, I are, however, good possible candidates. To ensure p-doping, an argument based on the balance between the cohesion energy of the dimers and the energy barrier for diffusion of the dopant is detailed. We believe that the achievement of p-doping as studied in this letter is not restricted to the particular case of the ZnO sodalite but can be generalized to other cage-like ZnO nanomaterials.

* Electronic address: dimitri.hapiuk@univ-lyon1.fr

[1] H. Hong, J. Shi, Y. Yang, Y. Zhang, J. W. Engle, R. J. Nickles, X. Wang, W. Cai, Nano Lett., **11**, 3744, (2011)
[2] S. Chu, G. Wang, W. Zhou, Y. Lin, L. Chernyak, J. Zhao, J. Kong, L. Li, J. Ren, J. Liu, Nature Nanotechnology **6**, 506, (2011)
[3] Ü. Özgür, Ya. I. Alivov, C. Liu, A. Teke, M. A. Reshchikov, S. Doŏan, V. Avrutin, S. J. Cho, and H. Morkoçd, J. of Appl. Phys. **98**, 041301 (2005)
[4] T. Tsukazaki, A. Ohtomo, T. Onuma, M. Ohtani, T. Makino, M. Sumiya, K. Ohtani, S.F. Chichibu, S. Fuke, Y. Segawa, H. Ohno, H. Koinuma, M. Kawasaki, Nat. Mat. **4**, 42 (2005)
[5] B. J. Morgan, Phys. Rev. B **80**, 174105 (2009)
[6] A. J. Kulkarni, M. Zhou, K. Sarasamak, and S. Limpijumnong, Phys. Rev. Lett. **97**, 105502 (2006)

[7] J. Carrasco, F. Illas, and S. T. Bromley, Phys. Rev. Lett. **99**, 235502 (2007)

[8] M. A. Zwijnenburg, F. Illas, and S. T. Bromley, Phys. Rev. Lett. **104**, 175503 (2010)

[9] D. Stradi, F. Illas and S.T. Bromley, Phys. Rev. Lett. **105**, 045901 (2010)

[10] F. Tournus, B. Masenelli, P. Melinon, D. Connetable, X. Blase, A. M. Flank, P. Lagarde, C. Cros, M. Pouchard, Phys. Rev. B, **69** , 035208 (2004)

[11] D. Connetable, V. Timoshevskii, B. Masenelli, J. Beille, J. Marcus, B. Barbara, A. M. Saitta, G.-M. Rignanese, P. Melinon, S. Yamanaka, X. Blase, Phys. Rev. Lett. **91**, 247001 (2003)

[12] D. Weaire and R. Phelan, Phil. Mag. Lett. **69**, 107 (1994)

[13] B. Wang, X. Wang, J. Zhao, J. Phys. Chem. C **114**, 5741 (2010)

[14] A. Dmytruk, I. Dmytruk, I. Blonsky, R. Belosludov, Y. Kawazoe, A. Kasuya, Microelectronics J. **40**, 218 (2009)

[15] R. Hoppe, E. Siepp, J. Solid State Chem. **72**, 52 (1988)

[16] G. Kresse and J. Furthmüller. Comput. Mat. Sci. **6** 15 (1996)

[17] J. P. Perdew, K. Burke, and M. Ernzerhof, Phys. Rev. Lett. **77** 3865 (1996)

[18] C. Friedrich, M. C. Müller, and S. Blügel, Phys. Rev. B **83**, 081101(R) (2011)

[19] M. Shishkin, and G. Kresse, Phys. Rev. B **75**, 235102 (2007)

[20] A. R. H. Preston, A. DeMasi, L. F. J. Piper, K. E. Smith, W. R. L. Lambrecht, A. Boonchun, T. Cheiwchanchamnangij, J. Arnemann, M. van Schilfgaarde, B. J. Ruck, Phys. Rev. B **83**, 205106 (2011)

[21] M. Stankovski, G. Antonius, D. Waroquiers, A. Miglio, H. Dixit, K. Sankaran, M. Giantomassi, X. Gonze, M. Côté, and G.-M. Rignanese, Phys. Rev. B **84**, 241201(R) (2011)

[22] P. E. Blochl. Phys. Rev. B, **50**, 17953 (1994)

[23] F. Bruneval, N. Vast, and L. Reining, Phys. Rev. B **74**, 045102 (2006)

[24] J. Vidal, S. Botti, P. Olsson, J.-F. Guillemoles, and L. Reining, Phys. Rev. Lett. **104**, 056401 (2010)

[25] J. Vidal, F. Trani, F. Bruneval, M. A. L. Marques, and S. Botti, Phys. Rev. Lett. **104**, 136401 (2010)

[26] X. Gonze, G.-M. Rignanese, M. Verstraete, J.-M. Beuken, Y. Pouillon, R. Caracas, F. Jollet, M. Torrent, G. Zerah, M. Mikami, Ph. Ghosez, M. Veithen, J.-Y. Raty, V. Olevano, F. Bruneval, L. Reining, R. Godby, G. Onida, D. R. Hamann, and D. C. Allan, Z. Kristallogr. **220**, 558 (2005)

[27] F. Trani, J. Vidal, S. Botti, and M. A. L. Marques, Phys. Rev. B 82, 085115 (2010)

[28] J. Vidal, F. Trani, F. Bruneval, M. A. L. Marques, and S. Botti, Phys. Rev. Lett. **104**, 136401 (2010)

[29] A. A. Demkov, O. F. Sankey, J.Gryko, and P. F. McMillan, Phys. Rev. B **55**, 6904 (1997)

[30] J. S. Kasper, P. Hagenmuller, M. Pouchard, and C. Cros, Science **150**, 11713 (1965)

[31] V. I. Smelyansky and J. S. Tse, Chem. Phys. Lett. **264**, 5, p.459-465 (1997)

[32] A. Ammar, C. Cros, M. Pouchard, N. Jaussaud, J. M. Bassat, G. Villeneuve, M. Duttine, M. Ménétrier, E. Reny, Solid State Sciences, **6**, 5, p. 393-400 (2004)